Toward broadband mechanical spectroscopy

Tina Hecksher[a,1], Darius H. Torchinsky[b,1,2], Christoph Klieber[c,1,3], Jeremy A. Johnson[c,1,4], Jeppe C. Dyre[a], and Keith A. Nelson[c,5]

[a]"Glass and Time," Department of Science and Environment, Roskilde University, DK-4000 Roskilde, Denmark; [b]Department of Physics, Massachusetts Institute of Technology, Cambridge, MA 02139; and [c]Department of Chemistry, Massachusetts Institute of Technology, Cambridge, MA 02139

Edited by Andrea J. Liu, University of Pennsylvania, Philadelphia, PA, and approved June 27, 2017 (received for review May 15, 2017)

Diverse material classes exhibit qualitatively similar behavior when made viscous upon cooling toward the glass transition, suggesting a common theoretical basis. We used seven different measurement methods to determine the mechanical relaxation kinetics of a prototype molecular glass former over a temporal range of 13 decades and over a temperature range spanning liquid to glassy states. The data conform to time–temperature superposition for the main (alpha) process and to a scaling relation of schematic mode-coupling theory. The broadband mechanical measurements demonstrated have fundamental and practical applications in polymer science, geophysics, multifunctional materials, and other areas.

viscous liquids | broadband mechanical spectroscopy | mode-coupling theory

The extraordinary slowing down of viscous liquid dynamics upon cooling toward the glassy state plays a key role in myriad contexts, including polymer processing, survival of living organisms in extreme cold, amorphous metal synthesis, and many others. Glass-forming liquids display a number of common features, despite quite different chemistry ranging from high-temperature covalently bonded glass formers to van der Waals liquids that typically form glasses below room temperature (1–6). This commonality makes the research area attractive from a theoretical point of view and motivates the detailed study of selected liquid systems in the hope of revealing generic features of glass-forming liquids.

Viscoelastic relaxation behavior derives from two distinct and sequential processes common to all glass-forming liquids. The primary or "alpha" structural relaxation dynamics, which dictate the time scales for molecular diffusion and flow, are nonexponential in time, typically extend over several decades of time scales at a single temperature, and shift dramatically from picoseconds at high temperatures and low viscosities to many seconds as the sample is cooled and the glassy state is approached. This behavior gives rise to broad loss peaks in elastic compliance spectra, covering an extended frequency range at any temperature and shifting from gigahertz to millihertz frequencies as the temperature is lowered (Fig. 1). In addition to the temperature-dependent alpha relaxation dynamics, local rearrangements of molecules within existing cage geometries of the molecules, the so-called (fast) "beta" relaxation processes, result in a higher-frequency feature in the loss spectrum.

This scenario applies in the simplest cases when structural relaxation is slowed down through obstruction among neighboring molecules as in van der Waals liquids but not through extensive networks as in hydrogen-bonded liquids or entanglements as in polymers. In general, additional so-called Johari–Goldstein beta processes are observed (7, 8). For the present study, we chose a liquid with no such additional processes, to make the analysis as simple as possible.

A variety of semiempirical models (9–14), as well as the first-principles mode-coupling theory (MCT) (15, 16), have been developed in an effort to rationalize supercooled liquid dynamics. In its idealized "schematic" form, MCT predicts, for the local density dynamics, a critical temperature T_c at which there is a transition from ergodic behavior above T_c to nonergodic behavior below, corresponding to arrest into a metastable glassy state.

A prominent feature in the last 50 years of discussions of viscous liquid dynamics is "time–temperature superposition" (TTS). TTS states that the alpha relaxation spectrum retains the same width and shape when the temperature is changed. A wide range of practices in polymer processing, rheology, aging, and other areas are based on TTS (17–21), but it has never been tested directly for mechanical properties across most of the time scales spanned. TTS forms the basis of many early heuristic descriptions of supercooled liquids extending from high temperature all of the way to the glass transition temperature; TTS is also predicted at $T > T_c$ by schematic MCT for the alpha process whenever it is well separated from the fast beta process (15, 16).

As input for theories of the dynamics of glass-forming liquids, information is needed over many decades of frequency (or time). Ideally, such broadband spectra should be taken for a large number of temperatures; this has been done spectacularly using dielectric relaxation spectroscopy, which covers an impressive 16 decades of frequency (22). Likewise, dynamic light scattering experiments cover 10 decades of frequencies (23). Unfortunately, neither technique monitors directly the density fluctuations, which, from a liquid-state theory viewpoint, are the most fundamental. Dielectric relaxation monitors the rotational degrees of freedom of polar molecules and molecular

Significance

Viscous liquids of all kinds, from honey to glycerol to common polymers, display remarkably similar dynamical properties upon cooling from high temperatures at which local structural relaxation and flow occur quickly, to moderate temperatures at which key components of the dynamics slow down dramatically, to cold temperatures at which a glassy solid is formed. The similarities suggest a common theoretical framework, but comprehensive measurements of liquids' mechanical properties covering the extraordinary range of time scales spanned have been elusive. Using seven experimental methods covering 13 decades with few gaps, we demonstrate that broadband mechanical spectra are now within reach. Data obtained for the molecular glass former studied, a commercial silicone oil, follow key scaling laws predicted long ago.

Author contributions: T.H., D.H.T., C.K., J.A.J., J.C.D., and K.A.N. designed research; T.H., D.H.T., C.K., and J.A.J. performed research; T.H., D.H.T., C.K., J.A.J., J.C.D., and K.A.N. analyzed data; and T.H., D.H.T., C.K., J.A.J., J.C.D., and K.A.N. wrote the paper.

The authors declare no conflict of interest.

This article is a PNAS Direct Submission.

[1]T.H., D.H.T., C.K., and J.A.J. contributed equally to this work.

[2]Present address: Department of Physics, Temple University, Philadelphia, PA 19122.

[3]Present address: Schlumberger, 92140 Clamart, France.

[4]Present address: Department of Chemistry and Biochemistry, Brigham Young University, Provo, UT 84604.

[5]To whom correspondence should be addressed. Email: kanelson@mit.edu.

This article contains supporting information online at www.pnas.org/lookup/suppl/doi:10.1073/pnas.1707251114/-/DCSupplemental.

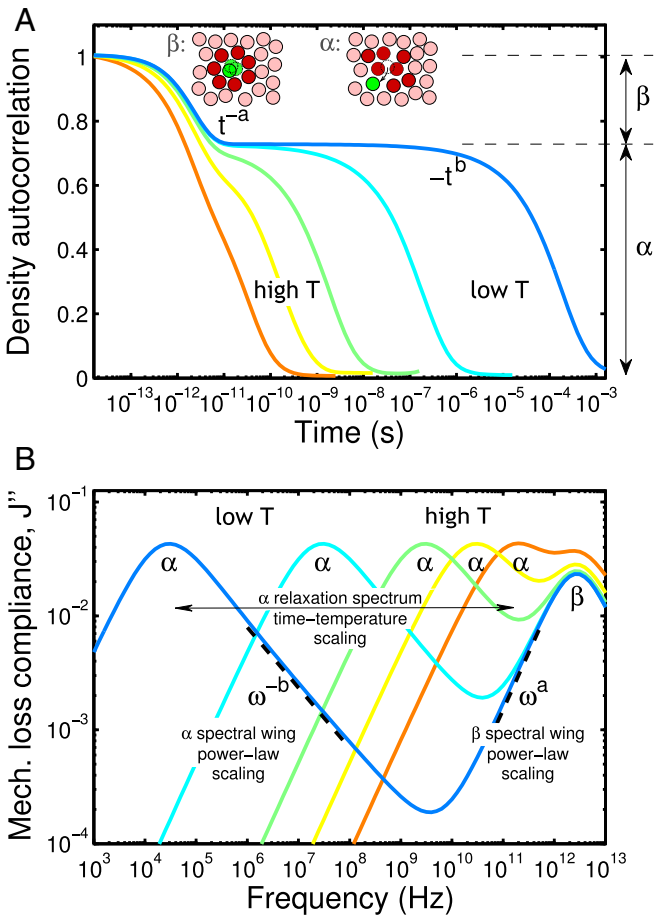

Fig. 1. Schematic depictions of primary alpha and faster beta relaxation processes in glass-forming liquids showing alpha and beta relaxation dynamics in (*A*) the time domain (via the density autocorrelation function) and (*B*) the frequency domain (via the elastic compliance loss spectrum). Time–temperature superposition is illustrated, as the alpha relaxation spectral shape and width remain constant while the frequency range shifts by many decades as the temperature is varied. Dynamic critical exponents *a* and *b* describe the asymptotic power-law scaling of the relaxation kinetics predicted by schematic MCT when the beta process (fast relaxation $\sim t^{-a}$ toward the constant plateau level) and the alpha process (slower relaxation $\sim -t^{b}$ decaying from the plateau level) are well separated. *Insets* in *A* show schematic representations of the beta relaxation among multiple potential energy minima (the different locations sampled by the central molecule colored green) within preexisting intermolecular "cages" formed by the red-colored molecules and alpha relaxation involving larger-scale rearrangement of the intermolecular geometries to permit molecular diffusion and flow.

groups, and dynamic light scattering monitors polarizabilities that include multiple contributions from which density dynamics are not easily extracted. What is needed are measurements of the temperature and frequency dependence of the elastic moduli over a large range of frequencies, which, via the fluctuation–dissipation theorem, relate directly to density and shear stress fluctuations. Due to various experimental challenges, such measurements have never been done over anywhere near the full frequency range of interest.

In this paper, we show how broadband mechanical spectra may be obtained by combining seven different recently developed techniques. The data are compared with TTS and with a scaling relation of schematic MCT, which has previously been tested through light and neutron scattering, as well as dielectric relaxation experiments (see, e.g., refs. 24–28), but not through direct measurement of density dynamics over a sufficient frequency range.

Experiments and Results

We used seven complementary methods, based on six experimental setups, to compile broadband longitudinal compliance spectra for the glass-forming liquid tetramethyl tetraphenyl trisiloxane (sold commercially as the diffusion pump oil DC704). Four of the methods were photoacoustic techniques (29–32) through which acoustic waves in the frequency range 1 MHz to 100 GHz were generated and detected optically. The corresponding acoustic wavelength range was ∼20 nm to 2 mm. Longer acoustic wavelengths are comparable to sample sizes, so, for lower frequencies in the range ∼1 mHz to 100 kHz, dynamical mechanical analysis methods involving piezoceramics that shear or compress the entire sample (33–35) were used. The measurements spanned more than 13 orders of magnitude in frequency with less than 3 decades of gaps, monitoring structural

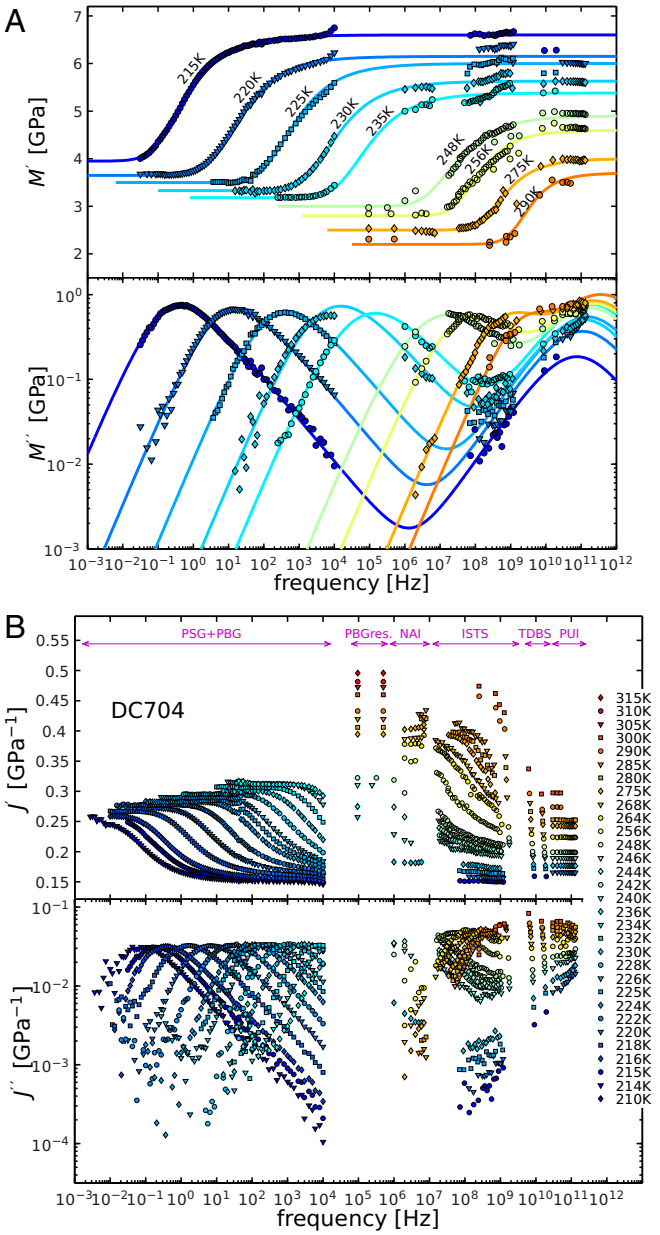

Fig. 2. (*A*) Longitudinal modulus spectra of DC704. Solid lines are guides to the eye. (*B*) Elastic compliance spectra of DC704. The techniques used in the different frequency ranges are indicated.

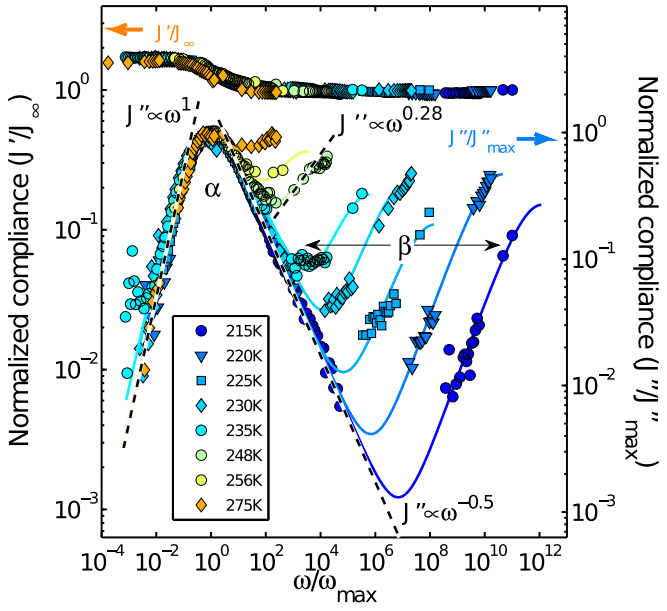

Fig. 3. Master plot of the compliance, demonstrating time–temperature superposition. The individual traces are scaled and shifted according to the fit values. The low-frequency side of the imaginary part follows a linear power law, $J'' \propto \omega^1$ (dashed line), corresponding to a simple exponential long-time decay of the stress autocorrelation function. The full curves give analytic model fits based on an alpha relaxation spectrum that follows an $\omega^{-0.5}$ high-frequency decay (compare *SI Appendix*, Fig. S18). The $\omega^{0.28}$ power law also shown here corresponds to the value found to fit the beta relaxation spectral wing near the minimum at 248 K (see Eq. **2** and Fig. 5).

relaxation dynamics in the temperature range 200 K to 320 K. Our earlier measurements in the low- and high-frequency ranges (33, 36) lacked sufficient frequency coverage for testing the MCT scaling prediction, but the gap was bridged by the newly developed Nanosecond Acoustic Interferometry (NAI) method. The experimental methods and data analysis through which we determined the compliance spectra and the elastic modulus (the inverse of the compliance) are described in *SI Appendix*.

Fig. 2 presents the complex longitudinal modulus and compliance spectra of DC704 in the frequency range of $\sim 10^{-3}$ Hz to 10^{11} Hz. The imaginary parts of the spectra have gaps in the ranges of $\sim 10^4$ Hz to 10^6 Hz and 1 GHz to 10 GHz. To facilitate visualization of the temperature-dependent trends, the modulus and compliance spectra show only a subset of the data collected.

The primary temperature dependence, observed clearly in both real and imaginary components of the modulus spectra, is the movement of the alpha relaxation peak across about 9 decades to lower frequencies as the temperature is reduced toward the glass transition temperature $T_g \approx 210$ K. At any given frequency ω_0, the real part of the modulus $M(\omega_0, T)$ increases as the sample is cooled, reflecting the stiffening of the liquid as it approaches the glassy state. At any given temperature T_0, the real part of the modulus $M'(\omega, T_0)$ plateaus at frequencies above those of the alpha relaxation spectrum, because, at such high frequencies, the liquid cannot undergo structural relaxation during the acoustic oscillation period, resulting in a solid-like response.

The compliance spectra show analogous behavior upon cooling: movement of the alpha relaxation spectrum across many decades and a decrease in the real part at low temperatures and high frequencies. The beta relaxation feature is observed most clearly in the imaginary parts of the modulus and compliance functions, which both rise at high frequencies.

TTS

As examples of the use of broadband mechanical spectra, we have compared the data to the predictions of TTS (this section) and schematic MCT (next section, *Testing a Scaling Prediction of Schematic MCT*). TTS states that, for the alpha relaxation dynamics, the normalized density autocorrelation function can be written as $\Phi(t, T) = F[t/\tau_\alpha(T)]$. In other words, TTS states that a single temperature-independent functional form $F[t/\tau_\alpha(T)]$ describes the relaxation dynamics at all temperatures, with the temperature dependence contained only in the values of the characteristic relaxation time $\tau_\alpha(T)$. In that case, the alpha relaxation compliance loss spectrum $J''(\omega)$ has a temperature-independent shape in a log–log plot.

To test TTS, we normalized the imaginary compliance spectra by the peak heights and normalized the real spectra by the high-frequency limiting value J_∞, and shifted both by amounts making the peak frequencies in $J''(\omega)$ coincide. The results are shown in Fig. 3. The alpha relaxation features superpose well across the entire temperature regime studied. The imaginary parts have the characteristic asymmetric shape found for most glass-forming materials: The low-frequency sides of the alpha relaxation spectra follow the Maxwell behavior, $J''(\omega) \propto \omega^1$, and the high-frequency sides follow a power law $J''(\omega) \propto \omega^{-1/2}$. The shifting of the spectra to make the alpha peaks overlap separates the beta relaxation features, which all appear at the high-frequency range in Fig. 2, on the scaled frequency axis. The scaled plots highlight the increase in separation between alpha and beta relaxations upon cooling.

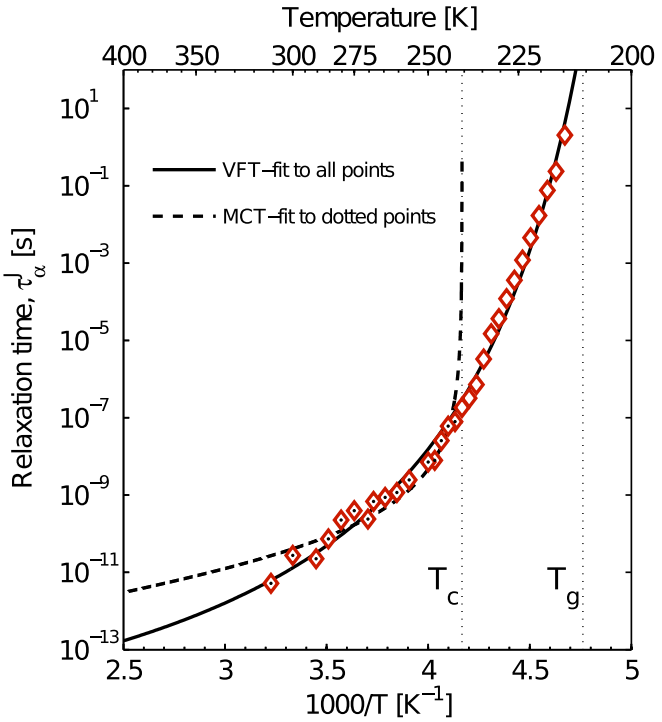

Fig. 4. The characteristic alpha relaxation time plotted as a function of inverse temperature where the Arrhenius equation gives a straight line. The glass transition temperature is $T_g \cong 210$ K. The VFT equation (*see Testing a Scaling Prediction of Schematic MCT*) was fitted to all data points (full line), yielding $\log \tau_0 = -15.0 \pm 0.8$, $D = 6 \pm 1$, and $T_0 = 183 \pm 5$ K. The MCT critical temperature $T_c = 240$ K was identified from Fig. 5*C* as the temperature below which MCT prediction breaks down; the MCT power law fit to the high-temperature points ($T > T_c$) (marked by central black dots) yielded the following fit parameters: $\log(\tau_x/\mathrm{s}) = -12.0 \pm 0.5$, $\gamma = 2.7 \pm 0.4$.

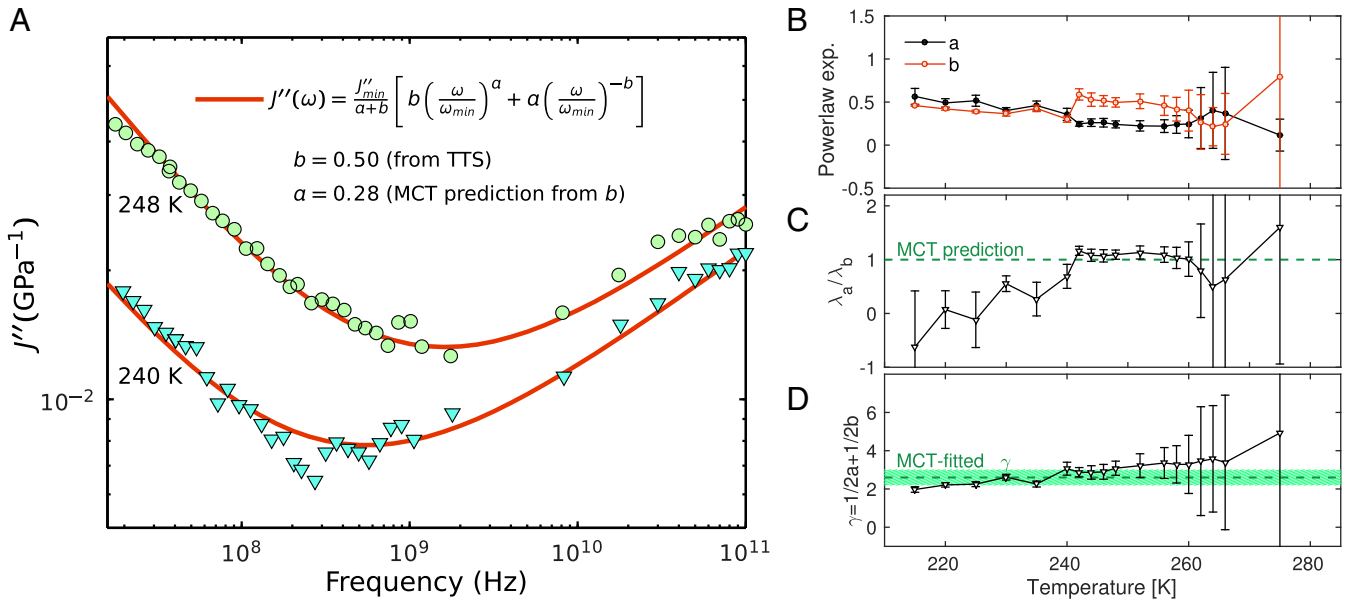

Fig. 5. (*A*) Data around the minimum of the imaginary part of the compliance function fitted to the MCT power-law relation, Eq. **2**, without adjustable shape parameters (critical exponents *a* and *b*) at sample temperatures of 240 K and 248 K. The exponent $b = 0.50$ was determined from the low-temperature data using TTS; Eq. **3** then yielded $a = 0.28$. (*B*) Values of power-law exponents *a* and *b* over a wide temperature range, determined as fitting parameters to Eq. **3**. (*C*) Test of the MCT prediction in Eq. **3** that $\lambda_a = \lambda_b$. The test is useful over the 240 K to 248 K temperature range. (*D*) The calculated exponent γ as a function of temperature. The green dotted line shows the value obtained from fitting Eq. **1** to the relaxation times (in *D*), and the green area gives the estimated uncertainty on this value.

Fig. 4 shows the values of the characteristic relaxation time τ_α of the alpha process as a function of temperature determined from fitting to the compliance data the Laplace transform of a stretched exponential function $\exp[-(t/\tau_\alpha)^n]$ with a temperature-independent stretching exponent n and strongly temperature-dependent τ_α values. The stretching exponent was fixed to $n = 0.5$, which, at high frequencies, corresponds to an $\omega^{-1/2}$ decay of the imaginary part of the compliance (4, 37, 38). The observed non-Arrhenius temperature dependence is typical of glass-forming liquids and is associated generally with a complex energy landscape rather than a single activation energy for all relaxation processes (2–6, 39).

Testing a Scaling Prediction of Schematic MCT

The relaxation time data were fit to the schematic MCT power-law prediction (15) of a divergence at a finite temperature (Fig. 4).

$$\tau_\alpha = \tau_x[T_c/(T - T_c)]^\gamma, \qquad [1]$$

with τ_x and γ as free parameters. This prediction is for temperatures above T_c (taken as 240 K as described below), although, as suggested heuristically, we find that TTS applies also below 240 K. The full set of $\tau_\alpha(T)$ values was fitted to the commonly used empirical Vogel–Fulcher–Tammann (VFT) function (40, 41) $\tau_\alpha(T) = \tau_0 \exp[DT_0/(T - T_0)]$. Although no divergence is observed, the temperature T_c at which the MCT prediction diverges is generally believed to define a temperature below which MCT breaks down because the physics changes into being dominated by hopping processes (15, 16).

A simple interpolation formula of the two power-law regimes predicted by schematic MCT (42),

$$J''(\omega) = \frac{J''_{min}}{a+b}\left[a\left(\frac{\omega}{\omega_{min}}\right)^{-b} + b\left(\frac{\omega}{\omega_{min}}\right)^{a}\right], \qquad [2]$$

connects the two relaxation features around the minimum between them. This expression was fitted to the measured spectra in the region around the minimum (Fig. 5*A*). The fitted values for a and b are shown in Fig. 5*B*. The uncertainty of the fits increases significantly as the temperature increases due to the merging of the two processes, making a distinction between the separate processes difficult. The MCT predicts a relation between the two exponents according to which

$$\lambda_a = \frac{\Gamma(1-a)^2}{\Gamma(1-2a)} = \lambda_b = \frac{\Gamma(1+b)^2}{\Gamma(1+2b)}, \qquad [3]$$

where $\Gamma(z)$ is the gamma function defined as $\Gamma(z) = \int_0^\infty x^{z-1}e^{-x}dx$. The relation is tested in Fig. 5*C*. The data are

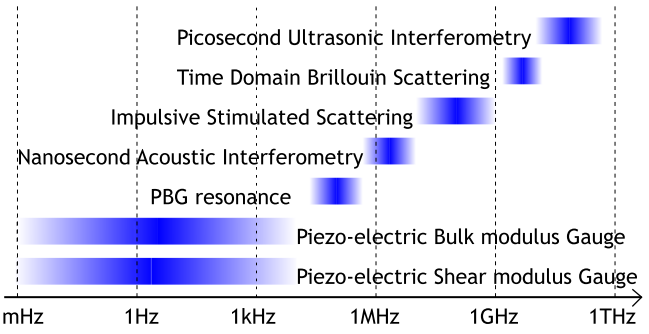

Fig. 6. Survey of mechanical spectroscopic techniques. At low frequencies (from megahertz up to ~10 kHz), the piezoelectric Shear modulus Gauge (PSG) and the piezoelectric bulk modulus Gauge (PBG) were used to measure the shear and bulk moduli. Analysis of the overtones in the PBG provided access to some data points in the 100- to 500-kHz region. In the low megahertz range, NAI was used to probe the frequency dependence of the longitudinal sound speed and attenuation rates directly. In the higher megahertz range, impulsive stimulated scattering (ISS) was used to measure longitudinal sound velocities and damping at specified acoustic wavevectors. Finally, time-domain Brillouin light scattering (TDBS) and picosecond ultrasonic interferometry (PUI) were used to measure longitudinal acoustic speeds and attenuation in the megahertz to gigahertz frequency ranges shown.

consistent with this prediction at temperatures above 240 K, but the relationship clearly breaks down below. We take this breakdown in the scaling relationship to define the critical temperature of schematic MCT, which is consistent with the fit of Fig. 4. Supporting this critical temperature assignment, the value of the alpha relaxation time at T_c, τ_α (240 K) $\approx$0.1 μs, is typical for T_c, below which the schematic MCT breaks down (16) due to the onset of thermally assisted hopping (43–45) through which alpha relaxation continues to occur.

Fig. 5*D* compares the alpha relaxation critical exponent γ determined in Fig. 4 based on $T_c = 240$ K to the MCT prediction that connects the power-law exponents to γ through the relation (15)

$$\gamma = 1/(2a) + 1/(2b). \quad \textbf{[4]}$$

The above analysis indicates that schematic MCT applies at temperatures above 240 K for DC704. For the fits to be useful as a test of the MCT predictions, there must be sufficient separation between the alpha and beta relaxation spectra as $T \to T_c$ from above that the a and b exponents can be associated distinctly with the two features (26, 46). The separation was sufficient for our results below 248 K, and thus MCT can be meaningfully tested in the temperature range 240 K to 248 K.

Fig. 5*A* shows the region around the minima between the alpha and beta features of the compliance loss spectra $J''(\omega)$ at temperatures 240 K and 248 K. As a final test, Eq. **2** was compared with the data with fixed exponent values. Only the minimum frequency $\omega_{\min}$ and the minimum compliance loss $J''_{\min}$ positions of each curve were adjusted to fit the data. The exponent value $b = 0.50$ was determined from the high-frequency wing of the alpha relaxation spectra evident in the TTS plot (Fig. 3). From this result, the predicted value of the exponent a could be calculated using Eq. **3**; this yielded the value $a = 0.28$, which should describe the low-frequency wing of the beta relaxation spectra. The resulting prediction completely determines the shape of the curves that go through the data well within the experimental scatter.

Conclusions

Our measurements demonstrate the feasibility of obtaining broadband mechanical relaxation spectra of a glass-forming liquid reaching the high frequencies of the beta relaxation spectrum and extending to the low frequencies of the alpha relaxation spectrum even as T_g is approached. The results give direct experimental support for TTS of the alpha relaxation spectrum, both above and below the critical temperature of schematic MCT (240 K), the validity of which is often assumed in empirical studies of glass-forming liquids and in modeling used for practical applications. Our results also permitted calculation of the dynamic critical exponents of schematic MCT above T_c, yielding results consistent with predictions that relate the alpha and beta relaxation dynamics. We also have measured shear relaxation dynamics across a wide frequency range (36), and filling in the frequency gaps for these measurements will permit comparison between longitudinal and shear dynamics that may show distinct temperature-dependent behavior (47).

DC704 is the first sample for which mechanical relaxation dynamics have been measured across the frequency range we have explored. Additional glass-forming liquids must be examined to assess the generality of TTS and MCT predictions. Our results demonstrate that access is now available to the extraordinarily wide frequency range needed for such comprehensive tests of supercooled liquids and a wide range of partially disordered materials including relaxor ferroelectrics, block copolymers, and many others. We hope the techniques are developed further in the future to make such measurements faster and less demanding. If and when this happens, it is realistic to imagine that broadband mechanical spectra will become as widely available as dielectric spectra are today.

Materials and Methods

Overview. The seven different measurement methods and the frequency ranges that they cover are summarized in Fig. 6; detailed descriptions of the techniques and data collected from them are discussed in *SI Appendix*. The techniques include three low-frequency methods involving piezoceramics that shear or compress the entire sample quasi-statically (33–35, 48) and four higher-frequency methods using short laser pulses to excite and subsequently detect acoustic waves in an irradiated region (30–32, 49–52).

The two lowest-frequency methods determine the complex frequency-dependent bulk modulus $K(\omega)$ and shear modulus $G(\omega)$ directly, where ω is the angular frequency. The longitudinal modulus is then given by $M(\omega) = M'(\omega) + iM''(\omega) = K(\omega) + (4/3)G(\omega)$. The four methods covering megahertz to gigahertz frequencies determine acoustic parameters. The complex longitudinal modulus is given from the acoustic data as $M(\omega, T) = \rho(T)(c_L(\omega, T))^2$, where $\rho(T)$ is the temperature-dependent density and $c_L(\omega, T)$ is the complex frequency-dependent longitudinal sound velocity.

To determine the modulus as a function of temperature from the sound velocity and damping rate, the thermal contraction of the sample must be accounted for. Using literature data of the thermal expansion coefficient $\alpha = 7.2 \times 10^{-4}[\mathrm{K}^{-1}]$ (53, 54) and assuming this quantity is temperature-independent, the following expression for the temperature dependence of the density can be derived (36):

$$\rho(T) = \frac{\rho(T_{ref})}{1 + \alpha_p(T - T_{ref})} = \frac{1.07[\mathrm{kg/m^3}]}{1 + 7.2 \times 10^{-4}[\mathrm{K}^{-1}]\,(\mathrm{T} - 298[\mathrm{K}])}. \quad \textbf{[5]}$$

Once the modulus is obtained, the complex longitudinal compliance is given by $J(\omega) = 1/M(\omega) = J'(\omega) - iJ''(\omega)$.

MCT relations are predictions for the mechanical susceptibility $\chi(\omega)$ to which $J(\omega)$ is proportional. Strictly speaking, $\chi(\omega)$ is related to the density autocorrelation function and therefore to the bulk compliance, not the longitudinal compliance. However, the difference between $K(\omega)$ and $M(\omega)$ (and thus also the bulk and longitudinal compliances) is very small because the shear modulus is considerably smaller than the longitudinal modulus, and their frequency-dependent dynamics are similar at both low (33, 55, 56) and high (47) frequencies.

Sample Preparation. For the PSG, PBG, and ISS measurements, DC704 was obtained from Sigma-Aldrich and used without purification. For the ISS measurements, the liquid was transferred into the cell through a 0.22-μm millipore filter into a fused quartz cuvette. During the ISS measurements, the sample was observed to become slightly opaque at the coldest temperatures; this is likely due to phase separation of dissolved impurities from the base liquid, and it disappeared when the liquid was reheated. The problem was overcome in subsequent experiments by mixing the sample with anhydrous $MgSO_4$, combined with heating under vacuum before filtration. This approach was adopted for the NAI, TDBS, and PUI techniques. Comparison of data both with and without treatment by the drying agent showed no difference in the acoustic parameters. The DC704 samples never crystallized during the course of our experiments.

The transducer techniques use home-built closed-cycle cryostats capable of keeping the temperature constant within a few milikelvins (57), and the NAI and ISS measurements were performed in a commercially available cold-finger cryostat. In these measurements, temperature sensing was provided by factory-calibrated platinum resistors immersed in the liquid a few millimeters away from the optical beams. The TDBS and PUI techniques were performed in a commercial sample-in-vapor cryostat, and the temperature was monitored at a position a few millimeters away from the sample.

We did not carry out any calibration of temperatures between the cryostats of the different laboratories. However, the low-frequency part of the longitudinal spectrum was obtained as the sum of two individual measurements that were carried out in the same experimental setup (same cryostat, same electronics). We estimate that the uncertainty on the absolute temperature is less than the overall noise in the high-frequency methods.

ACKNOWLEDGMENTS. The work at Massachusetts Institute of Technology was supported, in part, by National Science Foundation Grant CHE-1111557 and Department of Energy Grant DE-FG02-00ER15087. The work at Roskilde University was supported by Danish National Research Foundation Grant DNRF61 and by the VILLUM Foundation.

1. Kauzmann W (1948) The nature of the glassy state and the behavior of liquids at low temperatures. *Chem Rev* 43:219–256.
2. Angell CA (1995) Formation of glasses from liquids and biopolymers. *Science* 267:1924–1935.
3. Debenedetti PG (1996) *Metastable Liquids: Concepts and Principles* (Princeton Univ Press, Princeton).
4. Dyre JC (2006) Solidity of viscous liquids. IV. Density fluctuations. *Phys Rev E Stat Nonlin Soft Matter Phys* 74:021502.
5. Roland CM (2010) Relaxation phenomena in vitrifying polymers and molecular liquids. *Macromolecules* 43:7875–7890.
6. Berthier L, Biroli G (2011) Theoretical perspective on the glass transition and amorphous materials. *Rev Mod Phys* 83:587–645.
7. Johari GP, Goldstein M (1970) Viscous liquids and the glass transition. II. Secondary relaxations in glasses of rigid molecules. *J Chem Phys* 53:2372–2388.
8. Johari GP (1982) Effect of annealing on the secondary relaxations in glasses. *J Chem Phys* 77:4619–4626.
9. Dyre JC (2006) Colloquium: The glass transition and elastic models of glass-forming liquids. *Rev Mod Phys* 78:953–972.
10. Gibbs JH, DiMarzio EA (1958) Nature of the glass transition and the glassy state. *J Chem Phys* 28:373–383.
11. Cohen MH, Grest GS (1979) Liquid-glass transition, a free volume approach. *Phys Rev B* 20:1077–1098.
12. Kivelson D, Kivelson SA, Zhao XL, Nussinov Z, Tarjus G (1995) A thermodynamic theory of supercooled liquids. *Phys Stat Mech Appl* 219:27–38.
13. Jung Y, Garrahan JP, Chandler D (2005) Dynamical exchanges in facilitated models of supercooled liquids. *J Chem Phys* 123:084509.
14. Tripathy M, Schweizer KS (2009) The influence of shape on the glassy dynamics of hard nonspherical particle fluids. II. Barriers, relaxation, fragility, kinetic vitrification, and universality. *J Chem Phys* 130:244907.
15. Götze W, Sjögren L (1992) Relaxation processes in supercooled liquids. *Rep Progr Phys* 55:241–376.
16. Das SP (2004) Mode-coupling theory and the glass transition in supercooled liquids. *Rev Mod Phys* 76:785–851.
17. Ferry JD (1980) *Viscoelastic Properties of Polymers* (Wiley, New York).
18. Plazek DJ (1996) 1995 Bingham medal address: Oh, thermorheological simplicity, wherefore art thou? *J Rheol* 40:987–1014.
19. Olsen NB, Christensen T, Dyre JC (2001) Time-temperature superposition in viscous liquids. *Phys Rev Lett* 86:1271–1274.
20. Narayanaswamy OS (1971) A model of structural relaxation in glass. *J Am Ceram Soc* 54:491–498.
21. Moynihan CT, Easteal AJ, DeBolt M, Tucker J (1976) Dependence of the fictive temperature of glass on cooling rate. *J Am Ceram Soc* 59:12–16.
22. Lunkenheimer P, Schneider U, Brand R, Loidl A (2000) Glassy dynamics. *Contemp Phys* 41:15–36.
23. Petzold N, Rössler EA (2010) Light scattering study on the glass former o-terphenyl. *J Chem Phys* 133:124512.
24. Li G, Du WM, Sakai A, Cummins HZ (1992) Light-scattering investigation of α and β relaxation near the liquid-glass transition of the molecular glass salol. *Phys Rev A* 46:3343–3356.
25. Li G, Du WM, Chen XK, Cummins HZ, Tao NJ (1992) Testing mode-coupling predictions for α and β relaxation in $(Ca_{0.4}K_{0.6}(NO_3)_{1.4}$ near the liquid-glass transition by light scattering. *Phys Rev A* 45:3867–3879.
26. Götze W (1999) Recent tests of the mode-coupling theory for glassy dynamics. *J Phys Condens Matter* 11:A1–A45.
27. Wuttke J, et al. (1994) Neutron and light-scattering study of supercooled glycerol. *Phys Rev Lett* 72:3052–3055.
28. Shen GQ, et al. (2000) Experimental studies of the liquid-glass transition in trimethylheptane. *Phys Rev E* 62:783–792.
29. Yan Y-X, Nelson KA (1987) Impulsive stimulated light scattering. I. General theory. *J Chem Phys* 87:6240–6256.
30. Silence SM, Duggal AR, Dhar L, Nelson KA (1992) Structural and orientational relaxation in supercooled liquid triphenylphosphite. *J Chem Phys* 96:5448–5459.
31. Thomsen C, Grahn H, Maris H, Tauc J (1986) Surface generation and detection of phonons by picosecond light pulses. *Phys Rev B* 34:4129–4138.
32. Choi JD, Feurer T, Yamaguchi M, Paxton B, Nelson KA (2005) Generation of ultrahigh-frequency tunable acoustic waves. *Appl Phys Lett* 87:081907.
33. Hecksher T, Olsen NB, Nelson KA, Dyre JC, Christensen T (2013) Mechanical spectrum of viscous liquids. I. Low-frequency bulk and shear moduli of DC704 and 5-PPE measured by piezoceramic transducers. *J Chem Phys* 138:12A543.
34. Christensen T, Olsen NB (1994) Determination of the frequency-dependent bulk modulus of glycerol using a piezoelectric spherical shell. *Phys Rev B* 49:15396–15399.
35. Christensen T, Olsen NB (1995) A rheometer for the measurement of high shear modulus covering more than seven decades of frequency below 50 kHz. *Rev Sci Instrum* 66:5019–5031.
36. Klieber C, et al. (2013) Mechanical spectra of viscous liquids. II. Gigahertz-frequency longitudinal and shear acoustic dynamics in glycerol and DC704 studied by time-domain Brillouin scattering. *J Chem Phys* 138:12A544.
37. Barlow AJ, Erginsav A, Lamb J (1967) Viscoelastic relaxation of supercooled liquids. II. *Proc R Soc London, Ser A* 298:481–494.
38. Nielsen AI, et al. (2009) Prevalence of approximate $\sqrt{t}$ relaxation for the dielectric α process in viscous organic liquids. *J Chem Phys* 130:154508.
39. Böhmer R, Ngai KL, Angell CA, Plazek DJ (1993) Nonexponential relaxation in strong and fragile glass-formers. *J Chem Phys* 99:4201–4209.
40. Vogel H (1921) Das Temperaturabhängigkeitsgesetz der Viskosität von Flüssigkeiten. *Phys Z* 22:645–646.
41. Tammann G (1925) Glasses as supercooled liquids. *J Soc Glass Technol* 9:166–185.
42. Cummins HZ, et al. (1993) Light scattering spectroscopy of the liquid-glass transition: Comparison with idealized and extended mode coupling theory. *Phys Stat Mech Appl* 201:207–222.
43. Goldstein M (1969) Viscous liquids and the glass transition: A potential energy barrier picture. *J Chem Phys* 51:3728–3739.
44. Debenedetti PG, Stillinger FH (2001) Supercooled liquids and the glass transition. *Nature* 410:259–267.
45. Schroeder TB, Sastry S, Dyre JC, Glotzer SC (2000) Crossover to potential energy landscape dominated dynamics in a model glass-forming liquid. *J Chem Phys* 112:9834–9840.
46. Cummins H (1999) The liquid-glass transition: A mode-coupling perspective. *J Phys Condens Matter* 11:A95–A117.
47. Torchinsky DH, Johnson JA, Nelson KA (2012) α-scale decoupling of the mechanical relaxation and diverging shear wave propagation length scale in triphenylphosphite. *J Chem Phys* 136: 174509.
48. Hecksher T (2010) Relaxation in supercooled liquids: Linear and nonlinear, mechanical and dielectric studies of molecular liquids. PhD thesis (Roskilde Univ, Roskilde, Denmark).
49. Johnson JA (2011) Optical characterization of complex mechanical and thermal transport properties. PhD thesis (Mass Inst Technol, Cambridge, MA).
50. Yan Y-X, Nelson KA (1987) Impulsive stimulated light scattering. II. Comparison to frequency-domain light-scattering spectroscopy. *J Chem Phys* 87:6257–6266.
51. Torchinsky DH (2008) Optical study of shear and longitudinal acoustic waves and complex relaxation dynamics of glass forming liquids. PhD thesis (Mass Inst Technol, Cambridge, MA).
52. Klieber C (2010) Ultrafast photo-acoustic spectroscopy of super-cooled liquids. PhD thesis (Mass Inst Technol, Cambridge, MA).
53. Orcutt RH (1973) Interlot density variation of a siloxane manometer fluid. *J Vac Sci Tech* 10:506.
54. Poulter KF, Nash PJ (1979) Interferometric oil micromanometer. *J Phys E Sci Instrum* 12:931–936.
55. Christensen T, Olsen NB (1994) Quasistatic measurements of the frequency-dependent bulk and shear modulus of supercooled liquids. *J Non Cryst Solids* 172–174:362–364.
56. Gundermann D, Niss K, Christensen T, Dyre JC, Hecksher T (2014) The dynamic bulk modulus of three glass-forming liquids. *J Chem Phys* 140:244508.
57. Igarashi B, et al. (2008) A cryostat and temperature control system optimized for measuring relaxations of glass-forming liquids. *Rev Sci Instrum* 79:045105.